Nanoscale

Accepted Manuscript

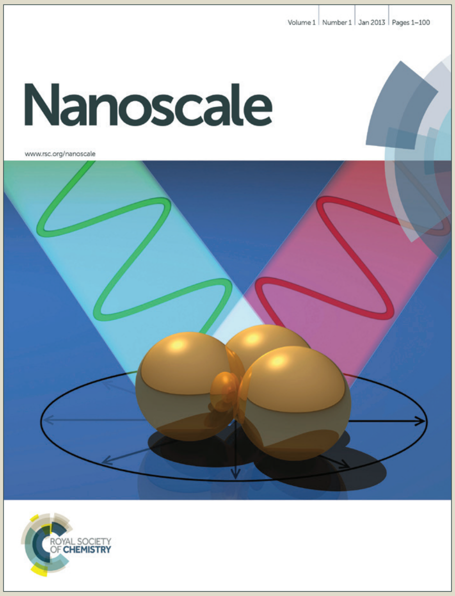

ROYAL SOCIETY OF CHEMISTRY

www.rsc.org/nanoscale

Ligand effect on isomer stability of $Au_{24}(SR)_{20}$ clusters

Qing Tang, Runhai Ouyang, Ziqi Tian, and De-en Jiang*

Department of Chemistry, University of California, Riverside, CA 92521, USA

*To whom correspondence should be addressed. E-mail: de-en.jiang@ucr.edu.

Abstract: A key challenge in nanocluster research in particluar and nanoscience in general is structure prediction for known compositions. Usually a simple ligand such as a methyl group is used to replace complex ligands in structure predicton of ligand-protected nanoclusters. However, how ligands dictate the energy landscape of such a cluster remains unclear. Here we elucidate the role of the ligand effect on the isomer stability of $Au_{24}(SR)_{20}$ nanocluster by computing the relative energy of two isomers (one from the experiment, denoted the “J” isomer; the other is the best theoretical model, denoted the “P” isomer) of $Au_{24}(SR)_{20}$ with dispersion-corrected density functional theory. We find that when R=-CH_3, the two isomers are equally stable (within 0.13 eV), but for R=-CH_2CH_2Ph, the P isomer is more stable by 1.6 eV while for R=-CH_2Ph-^tBu, the J isomer is more stable by 1.0 eV. Partition of the total energy into DFT and vdW contributions indicates that the higher stability of the P isomer in the case of R=-CH_2CH_2Ph stems from the stronger vdW interactions among -CH_2CH_2Ph groups, while the higher stability of the J isomer in the case of R=-CH_2Ph-^tBu is due to its better capacity to respond to the steric effect of the larger -CH_2Ph-^tBu groups. This finding confirms that the ligand plays a crucial role in dictating the isomer stablility.

TOC

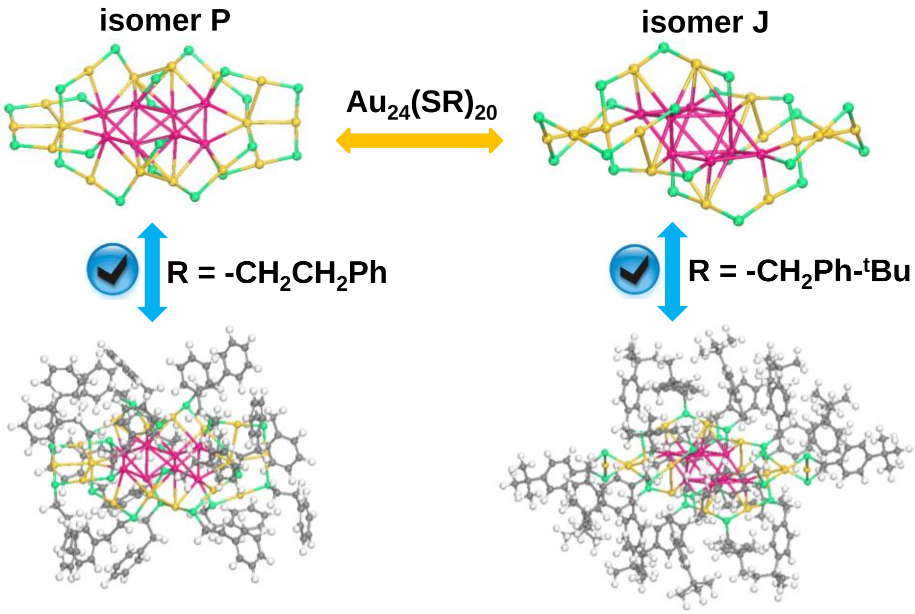

Ligands play an important role in stabilizing metal nanoclusters.[1,2] This is especially true in the case of thiolate-protected gold nanoclusters where many atomically precise compositions have been identified and more and more are structrue-determined.[3-11] However, it remains unclear how the ligand dictates the structure and stability of a cluster. In the extreme case of large, bulky ligands, the interfacial motif will change, so the composition will be different in terms of “magic” or special-stability clusters, as nicely demonstrated by Tsukuda and coworkers.[12] But for ligands of moderate bulkiness, one can obtain the same composition for different ligands. Whether or not the cluster has the same or different structure is an intriguing question. In other words, will the structure become different according to the ligand used, with the composition being the same? The relative stability of isomers may depend on the ligand. If this is indeed the case, then the implications on both synthesis and structure prediction are profound.

Density functional theory has been quite successful in predicting the structures of $Au_{25}(SR)_{18}^{-}$ [13] and $Au_{38}(SR)_{24}$ [14,15] and the majority of the computational studies simply uses CH_3 for R- for efficiency in exploring the relative stability of different isomers for a specific composition.[16-21] This simplification has an underlying assumption that the isomer stability does not depend on the R- group. Although this assumption has been challenged by recent computational and experimental studies,[10,22] to what extent this assumption is valid remains to be seen.

In this paper, we hypothesize that the isomer stability depends on the –SR group. This is motivated by the recent progress on the $Au_{24}(SR)_{20}$ clusters which provide a perfect case to test our hypothesis. In 2010, Zhu et al. synthesized and characterized $Au_{24}(SCH_2CH_2Ph)_{20}$, but its structure is still unknown.[23] Pei et al. searched structure models for the $Au_{24}(SCH_3)_{20}$ cluster and predicted that the lowest-lying structure (we call it the "P" isomer) corresponds to a prolate Au_8 core (two cross-joined tetrahedral Au_4 units with near-D_{2d} point group symmetry) capped by two sets of interlocked trimeric $[Au_3(SCH_3)_4]$ and pentameric $[Au_5(SCH_3)_6]$ motifs (as shown in Figure 1a), denoted as $Au_8[Au_3(SCH_3)_4]_2[Au_5(SCH_3)_6]_2$.[24] Interestingly, the P isomer has been confirmed to be the structure of $Au_{24}(SeR)_{20}$ nanocluster (R= $-C_6H_5$).[25] More recently, Jin et al. have solved the crystal structure of a $Au_{24}(SR)_{20}$ cluster, where R= $-CH_2Ph-^tBu$.[10] Different from the P model, $Au_{24}(SCH_2Ph-^tBu)_{20}$ features an anti-prismatic Au_8 core (with near-C_{2h} point group symmetry) protected by four tetrameric $Au_4(SR)_5$ motifs (shown in Figure 1b; we call it the "J" model). Hence the intriguing question is: Would the $Au_{24}(SCH_2CH_2Ph)_{20}$ cluster have the P structure or the J structure? In other words, when we switch the R- group from $-CH_2Ph-^tBu$ to $-SCH_2CH_2Ph$, does the structure change?

Another important factor about the ligand effect is the van der Waals (vdW) interaction. If $-SCH_3$ groups are used to replace the real or full experimental –SR groups for structure prediction, certainly the vdW interaction will be completely ignored. The role of the vdW interaction in dictating the isomer stability has not been fully quantified or clearly demonstrated. Recent experiment suggests that the vdW interaction is a key factor in facilitating formation of a polymer of $Au_{25}(SBu)_{18}$ clusters.[26]

Herein we seek to investigate the ligand effect on the isomer stabilities of $Au_{24}(SR)_{20}$ isomers via dispersion-corrected density functional theory (DFT) computations that incorporate vdW interactions into the DFT energetics, so that we can also quantify the role of the vdW interaction. Three types of ligands, R= $-CH_3$, $-CH_2CH_2Ph$, and $-CH_2Ph-^tBu$, are considered. All DFT calculations were done with the quantum chemistry program Turbomole V6.5.[27] Geometry optimizations of $Au_{24}(SR)_{20}$ isomers were performed using TPSS (Tao, Perdew, Staroverov, and

Scuseria) functional[28] for electron exchange and correlation and the def2-SV(P) basis sets. Note that PBE and the meta-GGA TPSS functionals were widely used for the geometric optimizations of $Au_n(SR)_m$ clusters.[24,29] TPSS has been shown to improve the calculated bond distances for $Au_{25}(SR)_{18}^-$ model systems.[30] The vdW interactions were included via the DFT-D3 method for structural optimizations of $Au_{24}(SCH_2CH_2Ph)_{20}$ and $Au_{24}(SCH_2Ph\text{-}^tBu)_{20}$ nanoclusters.[31] The power X-ray diffraction (XRD) patterns of the optimized structures were calculated by using the Debye formula. The diffraction intensity I(s) as a function of the diffraction vector length s ($s=2\sin\theta/\lambda$) is expressed as

$$I(s)=\sum_{i,j=1}^{N}\frac{cos\theta}{(1+\alpha cos^2 2\theta)}\exp(-\frac{Bs^2}{2})f_i f_j\frac{\sin(2\pi s r_{ij})}{2\pi s r_{ij}}$$

where θ is the diffraction angle, λ is the wavelength of the incident X-ray beam and is set as 1.542Å (Cu k_α X-ray source used in experiment[10,23]). The experiment-dependent parameter α is set to be 1.01. The r_{ij} is the distance between atom i and j, and (f_i, f_j) are the atomic scattering factors, which correspond to the atomic numbers. B is the damping parameter, which reflects the thermal effects, and is set as 0.005 nm^2.

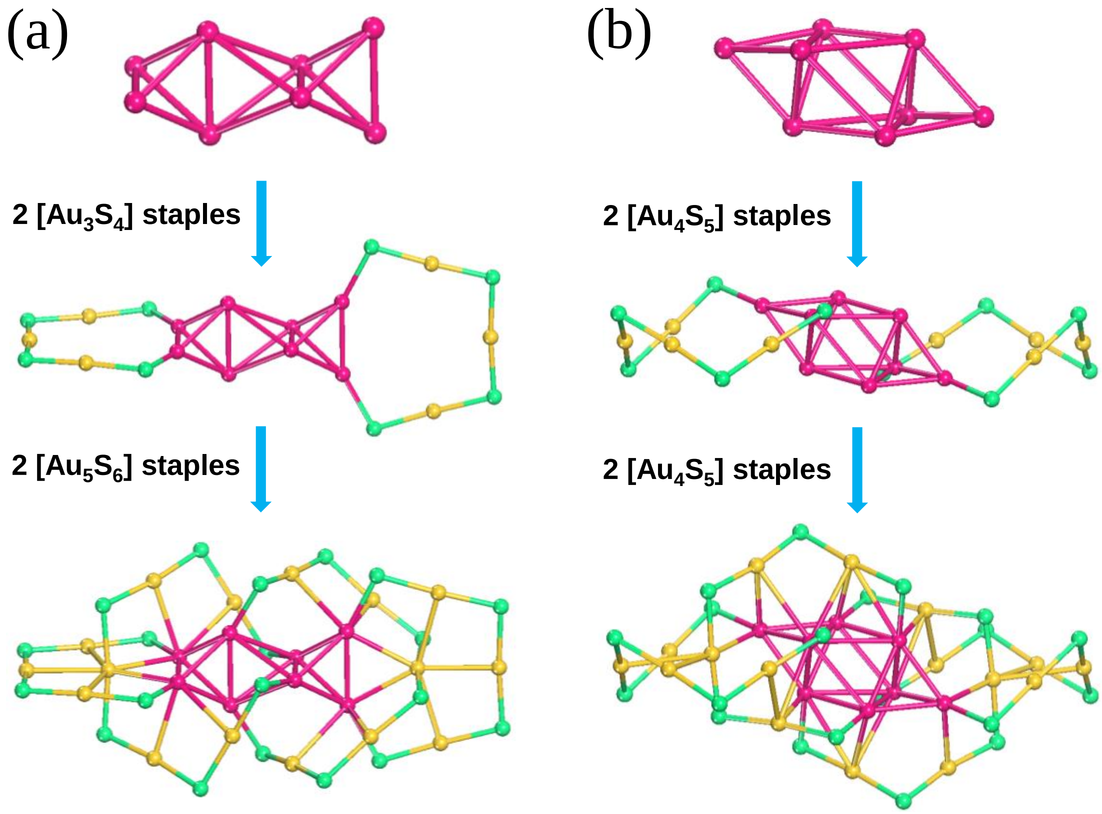

Figure 1. Frameworks of two $Au_{24}(SR)_{20}$ isomers: (a) a prolate Au_8 core and addition of two trimeric $Au_3(SR)_4$ staples and two pentameric $Au_5(SR)_6$ staples, written as $Au_8[Au_3(SR)_4]_2[Au_5(SR)_6]_2$ (isomer P); (b) an anti-prismatic Au_8 core and addition of four tetrameric $Au_4(SR)_5$ staples, written as $Au_8[Au_4(SR)_5]_4$ (isomer J). Color code: pink, kernel Au; yellow, staple Au; green: S; C and H not shown here.

We focus on the two isomers: P (Figure 1a) and J (Figure 1b) models. This is intended to specifically test our hypothesis that ligands dictate the relative stability of the isomers. Note that for the $Au_{24}(SR)_{20}$ cluster or any $Au_n(SR)_m$ cluster, each R group has two possible orientations (left or right of the S-Au-S plane), and so there are 2^{20} or 1,048,576 orientational conformations for both P and J isomers. It is prohibitive now to explore all of them. To do a computationally feasible configurational sampling, we first inspected the crystal structure of $Au_{24}(SePh)_{20}$[25] and

$Au_{24}(SCH_2Ph\text{-}^tBu)_{20}$[10] since the R groups of the experimentally obtained nanoclusters are in their optimal orientations. The $Au_{24}(SCH_2Ph\text{-}^tBu)_{20}$ J isomer is thus extracted directly from the crystal structure; by replacing all the -Ph-^{t}Bu tail groups with H and CH_2Ph, we get the initial structures for $Au_{24}(SCH_3)_{20}$ and $Au_{24}(SCH_2CH_2Ph)_{20}$ J isomers. For the P isomer, the best theoretical model by Pei et al.[24] for $Au_{24}(SCH_3)_{20}$ is used as an initial orientation; by replacing the CH_3 groups with CH_2CH_2Ph and $CH_2Ph\text{-}^tBu$ we then get $Au_{24}(SCH_2CH_2Ph)_{20}$ and $Au_{24}(SCH_2Ph\text{-}^tBu)_{20}$ initial orientations. Based on the initial structures of $Au_{24}(SCH_2CH_2Ph)_{20}$ (P and J isomers) and $Au_{24}(SCH_2Ph\text{-}^tBu)_{20}$ (P and J isomer), we then constructed about 10 to 16 orientational conformations for each of the three isomers by minimizing steric effect and maximizing symmetry from visual inspection. We also used classical molecular dynamics (MD) simulation with the Au-S framework fixed but allowing the –R groups to freely rotate from left to right (cis to trans) and generated 25 configurations from the MD trajectory for each of the four isomers. Geometry optimization of these conformations was first performed using the VASP code[32] at the DFT-PBE-D3 level[31,33] (the cluster was put into a $40\times40\times40$Å^3 box) for parallel efficiency and then the lowest-energy structures were re-optimized with Turbomole to avoid the periodic boundary conditions of VASP. Details of the configuration sampling, the orientational modes of some configurations, and their energies are shown in detail in Electronic Supplementary Information.

After structure sampling, the optimized lowest-energy structures of the two isomers for R= –CH_3, –CH_2CH_2Ph, and –$CH_2Ph\text{-}^tBu$ are shown in Figure 2. The atomic coordinates of these optimized structures are also listed in Electronic Supplementary Information. The close packing of surface ligands for $Au_{24}(SCH_2CH_2Ph)_{20}$ and $Au_{24}(SCH_2Ph\text{-}^tBu)_{20}$ isomers indicates substantial dispersion forces between the tail groups. The relative energies are shown in Table 1. For the small ligand (R=CH_3), the energy difference between isomer P and isomer J is small (0.13eV), implying that both isomers have comparable stabilities. For R=CH_2CH_2Ph, isomer P is also energetically more favorable by 1.60 eV, while for R=CH_2Ph-^tBu, the J isomer is more stable by 1.02 eV. This reversal of stability with a change of ligand confirms our hypothesis that the isomer stability depends on the ligand. It also indicates that the experimentally synthesized $Au_{24}(SCH_2CH_2Ph)_{20}$ cluster is likely to have a structure like that of the P isomer (Figure 2c). Additionally, we also used the non-local, electron-density dependent dispersion correction (vdW-DF)[34] to re-compute the energetics of the $Au_{24}(SCH_2CH_2Ph)_{20}$ and $Au_{24}(SCH_2Ph\text{-}^tBu)_{20}$ isomers. The vdW-DF computations give the qualitatively same energy orders as the DFT-D3 method. Furthermore, to check the influence of functional on the relative stability of $Au_{24}(SR)_{20}$ isomers, we used the PBE functional to re-examine the considered isomers. The PBE scheme predicts the same energetic order for the $Au_{24}(SCH_2CH_2Ph)_{20}$ and $Au_{24}(SCH_2Ph\text{-}^tBu)_{20}$ isomers as the TPSS functional.

Table 1. The energy difference between two $Au_{24}(SR)_{20}$ isomers (J and P) for different R groups. For R=CH_2CH_2Ph and CH_2Ph-^tBu, the energy difference is further broken down to DFT and vdW contributions. The HOMO-LUMO gaps (eV) are also shown.

$Au_{24}(SR)_{20}$	ΔE_{total} (eV)	ΔE_{dft} (eV)	ΔE_{vdw} (eV)	gap (eV)	
	$E_{total(J)}$-$E_{total(P)}$	$E_{dft(J)}$-$E_{dft(P)}$	$E_{vdw(J)}$-$E_{vdw(P)}$	isomer P	isomer J
R=CH_3	0.13	0.13	-	1.70	1.96
R=CH_2CH_2Ph	1.60	–0.72	2.32	1.63	1.90
R=CH_2Ph-^tBu	–1.02	–0.92	–0.10	1.75	1.93

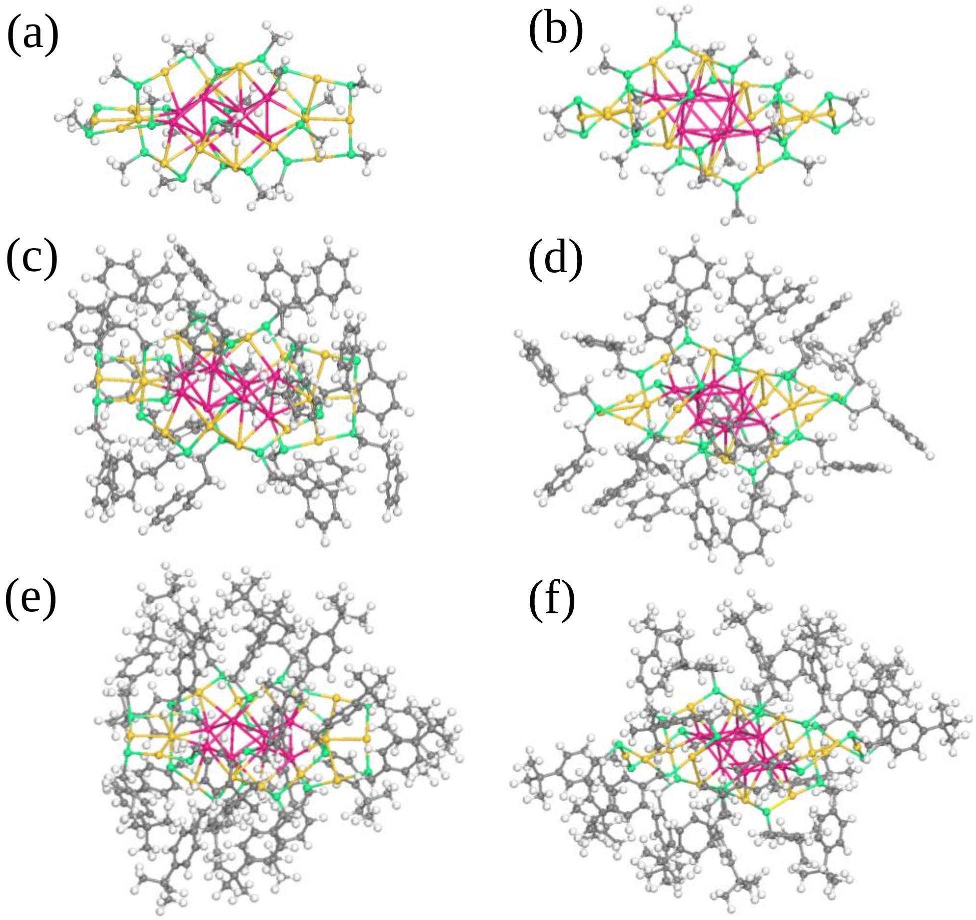

Figure 2. The optimized structures of $Au_{24}(SR)_{20}$ isomers for R = CH_3 (a, b), CH_2CH_2Ph (c, d), and CH_2Ph-^tBu (e, f). Left column corresponds to the isomer P; right column the isomer J.

To understand deeper the underlying reason for the change of stability, we break down the total energy into DFT and vdW contributions for $Au_{24}(SCH_2CH_2Ph)_{20}$ and $Au_{24}(SCH_2Ph\text{-}^tBu)_{20}$ nanoclusters. One can see that the preference of the P isomer in the case of R=CH_2CH_2Ph is clearly due to the much more favorable vdW interaction (by 2.32 eV) which overwhelms the penalty in DFT energy (by 0.72 eV). In the case of R=CH_2Ph-^tBu, the two isomers have almost the same vdW interaction, but the J isomer has a much lower DFT energy. The role of the vdW interaction in preferring the P isomer in the case of R=CH_2CH_2Ph is direct and clear. To gauge the contribution of the two different tail groups to the vdW interaction, we computed the average vdW energy per carbon atom ($\bar{E}_{\mathrm{vdw}}$) of $Au_{24}(SCH_2CH_2Ph)_{20}$ and $Au_{24}(SCH_2Ph\text{-}^{t}Bu)_{20}$ isomers (see Table 2). One can see that from R=CH_2CH_2Ph to R=$CH_2Ph\text{-}^{t}Bu$ for the same isomer, the vdW interaction is weakened, in agreement with the larger steric effect of the t-Bu group.

Table 2. The average vdW energy ($\bar{E}_{\mathrm{vdw}}$) per carbon atom of $Au_{24}(SCH_2CH_2Ph)_{20}$ and $Au_{24}(SCH_2Ph\text{-}^{t}Bu)_{20}$ isomers.

$Au_{24}(SR)_{20}$	$\bar{E}_{\mathrm{vdw}}$ (eV per carbon)	
	isomer P	isomer J
R=CH_2CH_2Ph	–0.195	–0.181
R=$CH_2Ph\text{-}^{t}Bu$	–0.178	–0.178

To understand why the J isomer is preferred in the case of R=$CH_2Ph\text{-}^{t}Bu$ while the two isomers have almost the same vdW energy, we analyzed how the core structure is changed upon switching R from –CH_3 to -$CH_2Ph\text{-}^{t}Bu$. We first examine the change in average Au-Au lengths of the Au_8 core. As shown in Table 3, the average core Au-Au bond length of the P isomer is contracted from 2.887Å for R=CH_3 to 2.863Å for R=$CH_2Ph\text{-}^{t}Bu$ (about 0.83% shrinkage). For the J isomer, the average core Au-Au bond is elongated slightly from 2.927Å for R=CH_3 to 2.932Å for R=$CH_2Ph\text{-}^{t}Bu$ (about 0.17% expansion). In other words, the bulky -$CH_2Ph\text{-}^{t}Bu$ group causes a greater perturbation to the core of the P isomer than to that of the J isomer. To further demonstrate this point, we replaced -$CH_2Ph\text{-}^{t}Bu$ in the relaxed $Au_{24}(SCH_2Ph\text{-}^{t}Bu)_{20}$ structures with –CH_3 and then fixed the $Au_{24}(SC)_{20}$ core; next we recomputed their energies. We find that the new $Au_{24}(SCH_3)_{20}$ structure is higher in energy than the original one by 1.60 eV for the P isomer and 1.25 eV for the J isomer. So indeed the bulky -CH_2Ph-^tBu group causes a greater energy penalty to the P isomer. In other words, the J isomer can better accommodate the bulky CH_2Ph-^tBu group. We think that this is the reason why the J isomer is preferred for R=CH_2Ph-^tBu.

Table 3. The average Au-Au bond length of Au_8 core for $Au_{24}(SR)_{20}$ P and J isomers.

Isomer	P		J	
R	CH_3	CH_2Ph-^tBu	CH_3	CH_2Ph-^tBu
core Au-Au (Å)	2.887	2.863	2.927	2.932

Another interesting question is how to differentiate isomer P and J to help the experimentalist determine which isomer would be the best candidate of a specific $Au_{24}(SR)_{20}$ cluster. To this end, we simulated the power X-ray diffraction patterns of the two $Au_{24}(SR)_{20}$ isomers for R=CH_2CH_2Ph (Figure 3). One can see that both isomers have rather similar patterns, but one can distinguish the two by the extra peak at ~48° for the P isomer. One can also distinguish the two isomers by their electronic structure. Table 1 shows that the calculated HOMO-LUMO gaps are within 1.63~1.75eV and 1.90~1.96eV for the P and J isomers, respectively. This indicates that one can potentially manipulate the geometrical and electronic properties of thiolated gold nanoclusters by controlling the ligands.

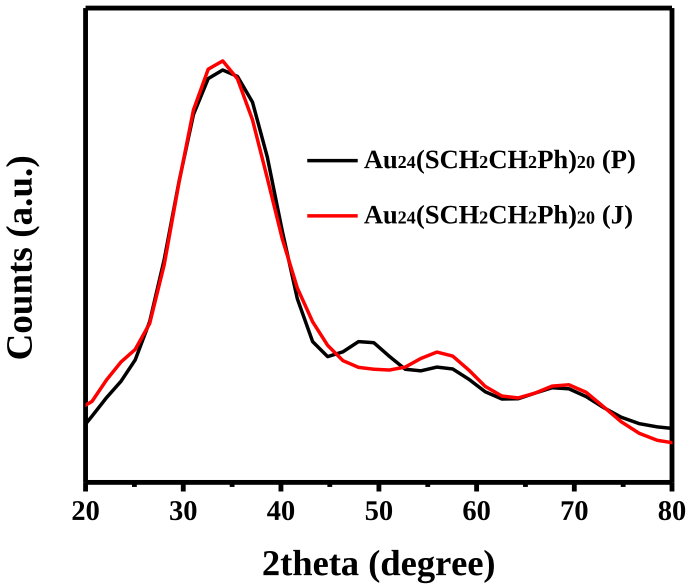

Figure 3. Simulated XRD patterns of $Au_{24}(SCH_2CH_2Ph)_{20}$ (P) and (J) isomers.

Considering the importance of ligands in dictating the isomer stability as demonstrated in this paper, one should now take the ligand seriously in structure prediction of $Au_n(SR)_m$ nanoclusters. For the sake of computational efficiency, it is perfectly fine to simplify the experimental R group to CH_3 at first, in order to quickly screen a lot of candidates with pure DFT (that is, without vdW interaction). However, one should then change CH_3 to the experimental R group and use dispersion-corrected DFT to re-optimize the structures and re-compare the relative energies for the low-lying isomers. It is especially important to follow this procedure for moderately bulky ligands such as $-SCH_2Ph-{}^tBu$.

In summary, we have studied the ligand effect on the isomer stability of $Au_{24}(SR)_{20}$ clusters with dispersion-corrected DFT, based on two candidate structures: isomer P, $[Au_8[Au_3(SR)_4]_2[Au_5(SR)_6]_2]$ and isomer J, $[Au_8[Au_4(SR)_5]_4]$. For $R=CH_3$, the two isomers have comparable energy (isomer P is slightly more stable by 0.13eV). For $R=CH_2CH_2Ph$, isomer P is energetically more favorable by 1.60 eV, mainly due to its much greater vdW interaction. For R=

CH_2Ph-${}^tBu$, the order is reversed and isomer J becomes more stable by 1.02 eV. In this case, the vdW forces have almost the equal contribution to the energetics of both isomers, and the higher stability of isomer J is attributed to its greater capacity to accommodate the perturbation to its core by the more bulky CH_2Ph-${}^tBu$ group. Hence the present work clearly demonstrated the role of ligands in dictating isomer stability and quantified the impact of the vdW interaction on the relative energetics. These insights will be useful in designing ligands to tune the geometric and electronic structures of ligand-protected metal clusters and in improving the protocol to more accurately predict their structures.

Acknowledgement. This work was supported by the University of California, Riverside. This research used resources of the National Energy Research Scientific Computing Center, a DOE Office of Science User Facility supported by the Office of Science of the U.S. Department of Energy under Contract No. DE-AC02-05CH11231.

References

1 R. C. Jin, *Nanoscale*, 2010, **2**, 343-362.

2 P. Maity, S. Xie, M. Yamauchi and T. Tsukuda, *Nanoscale*, 2012, **4**, 4027-4037.

3 Y. Negishi, K. Nobusada and T. Tsukuda, *J. Am. Chem. Soc.*, 2005, **127**, 5261-5270.

4 P. D. Jadzinsky, G. Calero, C. J. Ackerson, D. A. Bushnell and R. D. Kornberg, *Science*, 2007, **318**, 430-433.

5 M. W. Heaven, A. Dass, P. S. White, K. M. Holt and R. W. Murray, *J. Am. Chem. Soc.*, 2008, **130**, 3754-3755.

6 M. Zhu, C. M. Aikens, F. J. Hollander, G. C. Schatz and R. Jin, *J. Am. Chem. Soc.*, 2008, **130**, 5883-5885.

7 H. Qian, W. T. Eckenhoff, Y. Zhu, T. Pintauer and R. Jin, *J. Am. Chem. Soc.*, 2010, **132**, 8280-8281.

8 C. Zeng, H. Qian, T. Li, G. Li, N. L. Rosi, B. Yoon, R. N. Barnett, R. L. Whetten, U. Landman and R. Jin, *Angew. Chem. Int. Ed.*, 2012, **51**, 13114-13118.

9 C. Zeng, C. Liu, Y. Chen, N. L. Rosi and R. Jin, *J. Am. Chem. Soc.*, 2014, **136**, 11922-11925.

10 A. Das, T. Li, G. Li, K. Nobusada, C. Zeng, N. L. Rosi and R. Jin, *Nanoscale*, 2014, **6**, 6458-6462.

11 Y. Yu, Z. Luo, D. M. Chevrier, D. T. Leong, P. Zhang, D. E. Jiang and J. Xie, *J. Am. Chem. Soc.*, 2014, **136**, 1246-1249.

12 J. I. Nishigaki, R. Tsunoyama, H. Tsunoyama, N. Ichikuni, S. Yamazoe, Y. Negishi, M. Ito, T. Matsuo, K. Tamao and T. Tsukuda, *J. Am. Chem. Soc.*, 2012, **134**, 14295-14297.

13 J. Akola, M. Walter, R. L. Whetten, H. Häkkinen and H. Grönbeck, *J. Am. Chem. Soc.*, 2008, **130**, 3756-3757.

14 Y. Pei, Y. Gao and X. C. Zeng, *J. Am. Chem. Soc.*, 2008, **130**, 7830-7832.

15 O. Lopez-Acevedo, H. Tsunoyama, T. Tsukuda, H. Häkkinen and C. M. Aikens, *J. Am. Chem. Soc.*, 2010, **132**, 8210-8218.

16 H. Häkkinen, M. Walter and H. Grönbeck, *J. Phys. Chem. B*, 2006, **110**, 9927-9931.

17 Y. Pei and X. C. Zeng, *Nanoscale*, 2012, **4**, 4054-4072.

18 D. E. Jiang, *Nanoscale*, 2013, **5**, 7149-7160.

19 A. Tlahuice and I. L. Garzon, *Phys. Chem. Chem. Phys.*, 2012, **14**, 3737-3740.

20 D. E. Jiang, S. H. Overbury and S. Dai, *J. Am. Chem. Soc.*, 2013, **135**, 8786-8789.

21 Y. Pei, S. Lin, J. Su and C. Liu, *J. Am. Chem. Soc.*, 2013, **135**, 19060-19063.

22 C. Zeng, C. Liu, Y. Pei and R. Jin, *ACS Nano*, 2013, **7**, 6138-6145.

23 M. Zhu, H. Qian and R. Jin, *J. Phys. Chem. Lett.*, 2010, **1**, 1003-1007.

24 Y. Pei, R. Pal, C. Liu, Y. Gao, Z. Zhang and X. C. Zeng, *J. Am. Chem. Soc.*, 2012, **134**, 3015-3024.

25 Y. Song, S. Wang, J. Zhang, X. Kang, S. Chen, P. Li, H. Sheng and M. Zhu, *J. Am. Chem. Soc.*, 2014, **136**, 2963-2965.

26 M. De Nardi, S. Antonello, D. E. Jiang, F. Pan, K. Rissanen, M. Ruzzi, A. Venzo, A. Zoleo and F. Maran, *ACS Nano*, 2014, **8**, 8505-8512.

27 R. Ahlrichs, M. Bar, M. Haser, H. Horn and C. Kolmel, *Chem. Phys. Lett.*, 1989, **162**, 165-169.

28 T. Jianmin, J. P. Perdew, V. N. Staroverov and G. E. Scuseria, *Phys. Rev. Lett.*, 2003, **91**, 146401.

29 J.-Q. Goh, S. Malola, H. Häkkinen and J. Akola, *J. Phys. Chem. C*, 2013, **117**, 22079-22086.

30 J. Akola, K. A. Kacprzak, O. Lopez-Acevedo, M. Walter, H. Grönbeck and H. Häkkinen, *J. Phys. Chem. C*, 2010, **114**, 15986-15994.

31 S. Grimme, J. Antony, S. Ehrlich and H. Krieg, *J. Chem. Phys.*, 2010, **132**, 154104.

32 G. Kresse and J. Furthmuller, *Phys. Rev. B*, 1996, **54**, 11169-11186.

33 P. E. Blochl, *Phys. Rev. B*, 1994, **50**, 17953-17979.

34 O. A. Vydrov and T. Van Voorhis, *J. Chem. Phys.*, 2010, **133**.